TECHNICAL REPORT

SPACE TELESCOPE SCIENCE INSTITUTE
Operated for NASA by AURA

Title: NIRISS Dither Patterns for the WFSS and IMAGING observing modes	Doc #: JWST-STScI-004466, SM-12 Date: November 12, 2015 Rev: -
Authors: P. Goudfrooij and the NIRISS Operations Working Group Phone: 410 - 338 - 4981	Release Date: 11 December 2015

1 Abstract

We describe the scientific benefits of dither patterns developed for the WFSS and IMAGING observing modes of the Near-InfraRed Imager and Slitless Spectrograph (NIRISS). In doing so, we define and measure quantitative quality metrics for image quality, astrometry, and photometry on simulated NIRISS images for a variety of dither patterns and filters. We then compare the scientific benefits associated with the dither patterns with the observing overheads incurred by them to do a cost-benefit analysis. The general results are that short exposure sequences (or visits) of less than about 10,000 seconds of exposure time may benefit most from 2 to 4 sub-pixel dithers (depending on specifics of the observing program), while long exposure sequences of several 10^4 seconds of exposure time may benefit more from 9-12 sub-pixel dithers. We conclude by describing and tabulating the properties of the selected dither patterns for the WFSS and IMAGING modes.

2 NIRISS Observing Modes

NIRISS has 4 observing modes, which are tabulated below along with their main properties. Each of these observing modes map to an observation template for use in the Astronomer's Proposal Tool (APT). Operations concepts for the NIRISS GO observing modes are described elsewhere (Goudfrooij et al. 2013, 2014a,b, 2015).

Mode	Acronym	Main Properties
Wide-Field Slitless Spectroscopy	WFSS	R ~ 150; 0.8 – 2.5 μm
Single-Object Slitless Spectroscopy	SOSS	R ~ 700; 0.6 – 2.5 μm
Aperture Masking Interferometry	AMI	Optimized for $\lambda \geq 3.5$ μm
Imaging	IMAGING	Medium- and broad-band filters, 0.9-5 μm

3 Scope of this Study

The main purpose of this report is a study of the scientific benefits of a variety of dither patterns for the WFSS and IMAGING observing modes of NIRISS[1]. In doing so, we use the currently available knowledge about the geometric distortion of the NIRISS camera and the intra-pixel sensitivity of the HgCdTe flight detectors of JWST. The results of this study may prove useful in evaluating trade-offs between costs (e.g., overhead times associated with dithers) and benefits (e.g., improved image quality, astrometry, and photometry) for a given observing program with NIRISS.

4 Scientific Motivation for Dithering

The general science drivers for using dithers in the data taking of astronomical images have been described in detail in several previous studies (e.g., Lauer 1999a,b; Ferguson et al. 2000; Fruchter & Hook 2002; Koekemoer & Lindsay 2005). Here we only summarize these drivers in the context of the observing modes of NIRISS.

1. Dithering mitigates the effects of undesired detector features (e.g., blemishes such as bad pixels, coronagraphic spots and small scratches on the NIRISS pick-off mirror, etc.). Detector persistence or latency from previous exposures can also produce undesired features. If a target ends up on such a feature in one exposure, dithers can prevent them from also doing so in many other ones.
2. Dithering improves the effective sampling of the Point Spread Function (PSF) at wavelengths where the detector pixel size causes undersampling. Note that the NIRISS detector is critically sampled at ≈ 4 μm, near the long-wavelength end of the detector's sensitivity. Hence, for most NIRISS observations, the structure present in the astronomical scene is significantly undersampled. Dithering using fractional pixel offsets allows one to recover part of this structure.
3. Dithering mitigates the impact of flat-fielding errors on (spectro-)photometry. By placing each target onto different pixels in different exposures, each exposure will suffer a different flat-field error. Due to Poisson statistics, the average of N_{DITH} dithered exposures will therefore have a flat-fielding error reduced by a factor $\sqrt{N_{\mathrm{DITH}}}$.
4. Similarly, dithering also improves the noise properties of images corrected for geometric distortion. Distortion correction of a stack of images taken with one pointing will suffer from severe correlated sampling errors. A stack of dithered images will mitigate such errors.
5. Dithering mitigates the variation in sensitivity across *individual* detector pixels. In undersampled images with HgCdTe detector arrays such as the NIRISS detector, one of the dominant sources of photometric and astrometric error is due to sensitivity variations across pixels, which is often quantified by the so-called intra-pixel sensitivity (IPS) response function (see, e.g., Lauer 1999b). The

[1] The dither patterns for the NIRISS/AMI mode will be described in detail elsewhere, since they serve a somewhat different purpose than those for the WFSS and IMAGING modes.

severity of this effect scales with the level of undersampling, and will thus be especially significant at $\lambda < 2$ μm for NIRISS observations of point (or compact) sources. Dithering using fractional pixel offsets can reduce this effect by a factor $\sqrt{N_{\mathrm{DITH}}}$ (in the case of sky-limited observations).

6. Dithering can be used to correct for temporal variations in the background level (and its negative effect on photometric accuracy). Such variations can result from scattered light from bright objects (be it sources on the detector or outside the field of view), instrument ghosts, detector persistence or latency, and/or time-dependent thermal glow from instrument electronics or the telescope. Such effects can be mitigated by using dithers on spatial scales similar to the typical target diameter (or, for the case of slitless spectroscopy like the WFSS observing mode, the target extent in the cross-dispersion direction).

Given these several benefits, dithering will be required for observations in almost all NIRISS observing modes. The only NIRISS observing mode for which dithering will *not* be implemented is the single-object slitless spectroscopy (SOSS) mode, which is focused on high-precision differential spectrophotometry of relatively bright targets (such as transit studies) and where the goal is to minimize any and all possible systematic differences between individual exposures in a sequence (and even between exposures of different targets; see Goudfrooij et al. 2014b, 2015). Observations in all other NIRISS modes will be required to use dithering, which will therefore be an integral aspect of observing programs. As such, the total exposure time for a given NIRISS observing sequence will be fully defined by three parameters: (1) the readout (sub)-array, (2) the dither pattern, (3) the MULTIACCUM parameters of the exposure (i.e., number of frames per readout, number of readouts per integration and number of integrations per exposure). The chosen dither pattern will directly map to the number of exposures used, while the combination of the readout (sub-)array and the MULTIACCUM parameters will set the exposure time per exposure.

JWST users will have to choose among a restricted set of (pre-set) dither patterns for a given observing mode. This contrasts with the situation for HST observations, where users are allowed to design their own dither patterns or even forego dithering completely (although the latter has generally been strongly discouraged for several years now). The reason for this significant change from HST operations is two-fold. The new dithering policy will allow the calibration pipeline to be fine-tuned for each dither pattern, so that the resulting data products will be of uniform and high quality. This will not only benefit the observer, it will also ensure the legacy of JWST data quality for future archival studies.

5 Evaluating NIRISS Dither Patterns

5.1 General considerations regarding dither patterns for NIRISS

The NIRISS detector is a HgCdTe chip with 2048×2048 pixels manufactured by Teledyne. The detector pixel size is ~ 65 milli-arcsec (mas) per axis, for which JWST provides Nyquist sampling at 4.0 μm. Since NIRISS observing modes cover wavelengths from 0.6 to 5 μm, several NIRISS observations will suffer from undersampling. This will

be true in particular for the Wide-Field Slitless Spectroscopy (WFSS) mode of NIRISS (Goudfrooij et al. 2013), which involves imaging and low-resolution spectroscopy at wavelengths $0.8 < \lambda/\mu m < 2.3$. As such, a significant component of the present study involves an investigation of the ability of sub-pixel dithers in recovering the intrinsic PSF as a function of wavelength for the WFSS and IMAGING observing modes. This is done by means of simulations that are described below in §§5.2 – 5.4. Dithering in the context of the Aperture Masking Interferometry (AMI) mode of NIRISS will be described in a separate report.

5.2 Image combination method

To evaluate the cost-benefit relation for dither patterns, we combine individual images of a dithered set by means of the linear image reconstruction algorithm "drizzle" (Fruchter & Hook 1997, 2002), which has been used for this purpose in the HST data reduction pipeline for images taken with the ACS and WFC3 cameras for several years now. If a sufficient number of dithered images are taken with carefully selected sub-pixel offsets, the "drizzle" algorithm is in principle able to reach a spatial resolution equal to the convolution of the PSF with the detector pixel scale. We note that other techniques can in principle improve the resolution even further. Such "image *restoration*" techniques are in general conceptually different from image *reconstruction* in that they aim to improve spatial resolution by taking into account high-frequency Fourier components of the observed images. An example of this technique in the context of combining dithered images is the Fourier reconstruction method of Lauer (1999a). While such techniques can be very powerful for specific applications, they do involve a trade-off between signal-to-noise (S/N) ratio and spatial resolution in their output images. To avoid lengthy iterative processing in that context, we chose to use the "drizzle" method that does not involve sacrifices for S/N ratio and for which the behavior of systematic errors is well understood.

5.3 Creation of simulated images

5.3.1 Dither Patterns used in Simulations

Simulations were carried out by placing a grid of PSFs across a detector pixel array. The PSFs were placed on the individual pixel arrays (i.e., the individual exposures) according to the pixel shifts associated with various sub-pixel dither patterns that range from a simple 2-point pattern to a full 9-point (3×3) sub-pixel grid. These dither patterns are listed in Table 1, along with the drizzle parameters used to produce the combined images. These drizzle parameters were chosen to optimize spatial resolution for each pattern and were based on the recommendations in the DrizzlePac handbook (Gonzaga et al. 2012) as well as past experience with the drizzle algorithm. The pixel shifts in Table 1 were chosen with the following general goals in mind:

1. The fractional pixel shifts were chosen to sample 2-D pixel phase in an optimal way (for the number of dithers in the dither pattern in question).
2. Use dither step amplitudes large enough to step over the spatial extent of the PSFs and the typical extent of blemishes and structures in the bias level or dark current of the detector, but otherwise as small as possible. The latter is done to minimize the impact of geometric distortion in terms of conserving pixel phase sampling

across the field of view.

3. Avoid multiple positions on the same detector rows and columns. This was done to minimize the effects of systematic offsets of columns or rows.

Table 1 Dither patterns and drizzle parameters used in simulations

Pattern	Pixel shifts (x, y)	Drizzle Parameters	
		Output Pixel Scale	Output 'pixfrac'
2-point	(0.0, 0.0) (4.5, 4.5)	0.5	1.0
3-point	(0.0, 0.0) (4.33, 4.33) (8.67, 8.67)	0.5	1.0
4-point	(0.0, 0.0) (5.0, 2.5) (2.5, 6.0) (−2.5, 4.5)	0.5	0.8
9-point	(4.00, 6.67) (7.33, 8.67) (10.67, 10.67) (2.00, 3.33) (5.33, 5.33) (8.67, 7.33) (0.00, 0.00) (3.33, 2.00) (6.67, 4.00)	0.5	0.8

5.3.2 Properties of Simulated Images

Direct imaging PSFs for each NIRISS filter were created using 11-fold oversampling of detector pixels, using M. Perrin's WebbPSF package (Perrin et al. 2014). The latter utilizes a model of the telescope and instrument optics, including the effect of optical path differences (OPDs) between the individual JWST mirror segments. We assumed an OPD of 162 nm RMS for these simulations.

For each dither pattern, a series of dithered exposures were created of a regular 10x10 grid of artificial stars across the detector. Before adding the stars to the images, two additional spatial offsets were applied to each star:

1. An offset equal to that induced by the modeled geometric distortion of the NIRISS detector at the location of the star. Geometric distortion properties of the NIRISS detector were taken from Martel & Fullerton (2013) in the form of polynomial coefficients that were tabulated and used in image combination with the drizzle algorithm.
2. A random offset *to each individual star* in the range 0 − 1 pixel in both X and Y. This was done (through WebbPSF) to simulate the effect of stars falling on random locations within a pixel. A given star got the same spatial offset applied in each of the dithered images of a dither pattern.

The background level in the simulated images was assumed to be that appropriate for a total exposure time of 5000 s, divided evenly among the individual exposures in a dither pattern. These background levels were estimated for every filter using the NIRCam module of the prototype exposure time calculator available on the STScI website. Stars were allocated a flux that yields S/N = 30 for aperture photometry with a radius of 3 pixels. Poisson noise was added to each image prior to image combination.

5.3.3 Implementation of Intra-Pixel Sensitivity Variations

For the current simulations, we adopted the results of Hardy et al. (2014) who performed measurements of the intra-pixel sensitivity (IPS) variations of a Teledyne HgCdTe detector similar to the flight detectors used on the near-IR instruments on JWST. We

modeled their results on the sensitivities *S* of *individual* pixels[2] by means of a quadratic function $S = 1 - (1 - a)r^2$ where *a* is the sensitivity at the pixel corner and *r* is the distance from the center of a pixel in units of the semi-diagonal of a pixel. This function is applied to each pixel individually by selecting a value for *a* from a normal distribution with $\mu_a = 0.80$ and $\sigma_a = 0.05$. We sampled the IPS function by subsampling detector pixels by a factor 11 in each axis, the same oversampling as that used to create the PSFs. The sensitivities of the individual pixel were subsequently normalized to unity. After multiplying the input (oversampled) PSFs by the IPS map, pixels were rebinned to native detector pixels and inserted into the full images. For comparison purposes, all simulated images were created twice: once with IPS variations and once without.

5.3.4 Image Combination

Each set of simulated dithered images was combined by means of the PyRAF task MultiDrizzle (Koekemoer et al. 2002). To do so successfully, it was necessary to use specific header keywords and image extensions that are used for HST instruments with near-IR detectors. We therefore used the FITS header keywords and image extensions from a WFC3/IR image as a template and changed the values of the following header keywords: IDCTAB, ADCGAIN, EXPEND, CRPIX1, CRPIX2, CD1_1, CD1_2, CD2_1, CD2_2, SAMP_SEQ, NSAMP, CENTERA1, CENTERA2, SIZAXIS1, SIZAXIS2, NAXIS1, NAXIS2. Correction for the spatial offsets between the individual images in a dither pattern was done by means of "shift files" (see Chapter 5.5.2.3 in Fruchter et al. 2009).

Figure 1 depicts a comparison between input and output images in the case of a simulated point source in the F200W filter, using the 4-point dither pattern listed in Table 1. Note that the pixel scale of the output image is 0.5 times that of the input images. The top left panel of Figure 1 depicts the first exposure, in which the PSF was chosen to be centered on a pixel. The fact that its central 4 pixels stand out in terms of their flux reflects the fact that F200W images are undersampled on the NIRISS detector by a factor of ~2. Note also the significantly improved sampling in the output image (see bottom two panels).

5.4 Analysis of Combined Output Images

After all the drizzled output images were created for all sets of dither patterns and NIRISS filters, the photometric and astrometric properties of the stars were measured. We concentrated on three "quality measures" of the resulting stellar data, namely their FWHM values, magnitudes, and positions. The latter two parameters were measured using the DAOPHOT/APPHOT package (Stetson 1987) in multi-aperture photometry mode. Stellar positions were measured using centroids (i.e., intensity-weighted means of the radial stellar profiles in x and y) while the FWHM measurements were done using the `psfmeasure` task within IRAF/PyRAF in "direct FWHM" mode. This task performs a

[2] Hardy et al. (2014) suggest that the loss of sensitivity towards the edges and corners of individual pixels seen in their tests are due to photons being redistributed to neighboring pixels. When they average over an array of 3×3 pixels, they find no detectable drop at the pixel edges. As such, the results from our IPS tests should be interpreted as "worst-case" results. Calibration images to be taken during Cryogenic Vacuum test #3 (CV3) at GSFC will allow us to evaluate the actual level of IPS variations in the NIRISS flight detector.

direct measure of the (interpolated) radial profile of the PSF, thus avoiding the need to assume a functional form for the latter (which often introduces systematic effects).

For the FWHM, the quality metric was chosen to be the measured value divided by the theoretical "ideal" value for critical sampling at the central wavelength of the filter in question (i.e., 1.22 λ/D). This ratio therefore provides a measure of how well the PSF is sampled by the output pixel grid relative to the case where the PSF is critically sampled.

For the astrometric and photometric measurements, the quality metric was defined as the standard deviation among the individual stars (which all had the same input magnitude). Magnitudes were measured within a radius of 3 pixels from the measured PSF center for this purpose. For the astrometry, the standard deviations were evaluated among the differences between the measured positions and the (known) input positions. The latter were determined using the PyRAF task `tran`.

For each of the dither patterns and filters, the resulting metrics for the FWHM, astrometry, and photometry are depicted in Figures 2 and 3.

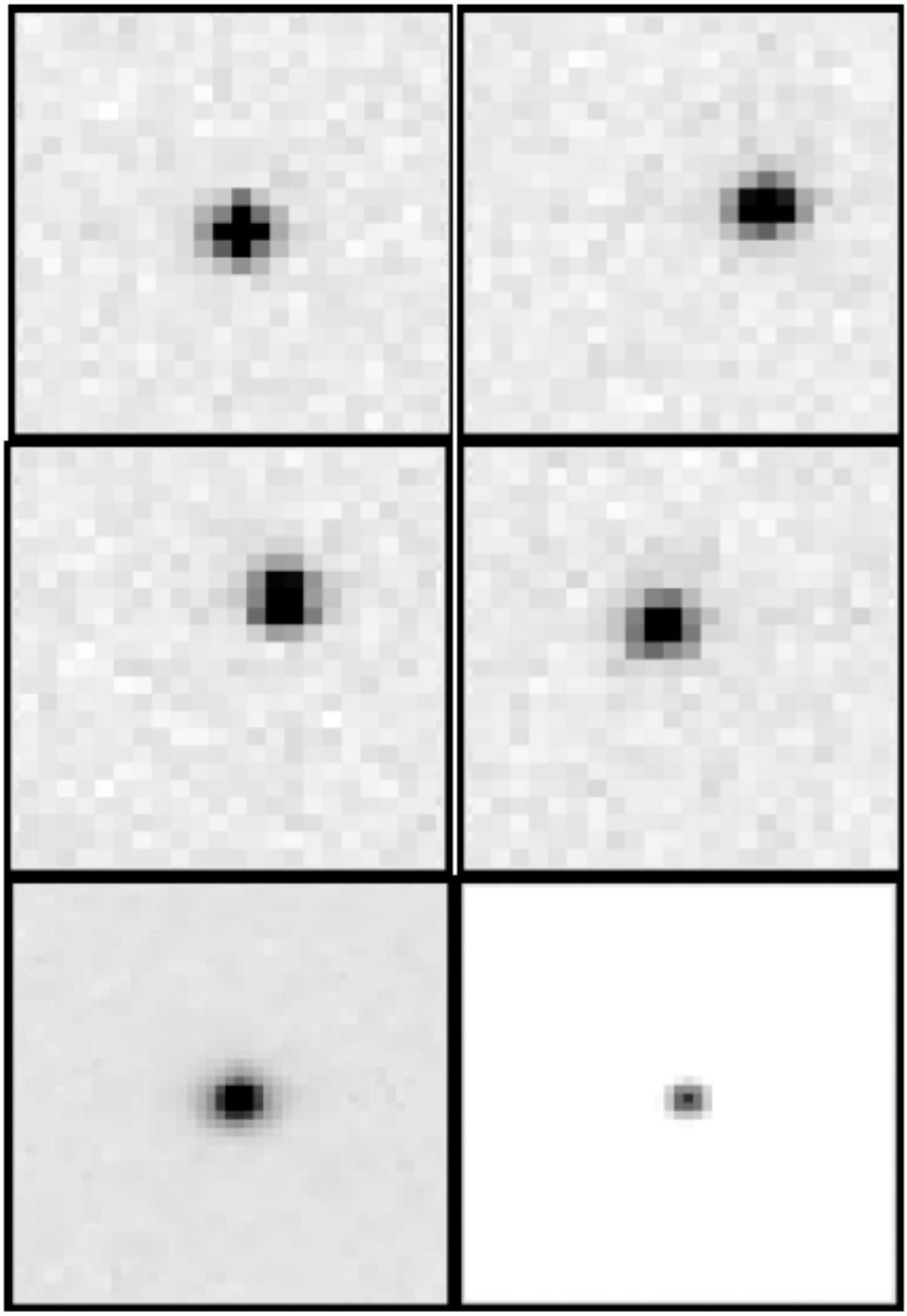

Figure 1: Example of a simulated 4-point dithered exposure of a point source imaged with the F200W filter of NIRISS. The top 4 panels show the 4 individual (dithered) input exposures, which include sky background, dark current, and Poisson noise. The bottom 2 panels depict the output drizzled image (at half the input pixel scale), at two different grey scale stretches: the bottom left panel has the same stretch as the 4 input images while the stretch of the bottom right panel was chosen to reveal the improved sampling in the PSF core. All panels show the same area on the detector in the native (input) pixel coordinate system.

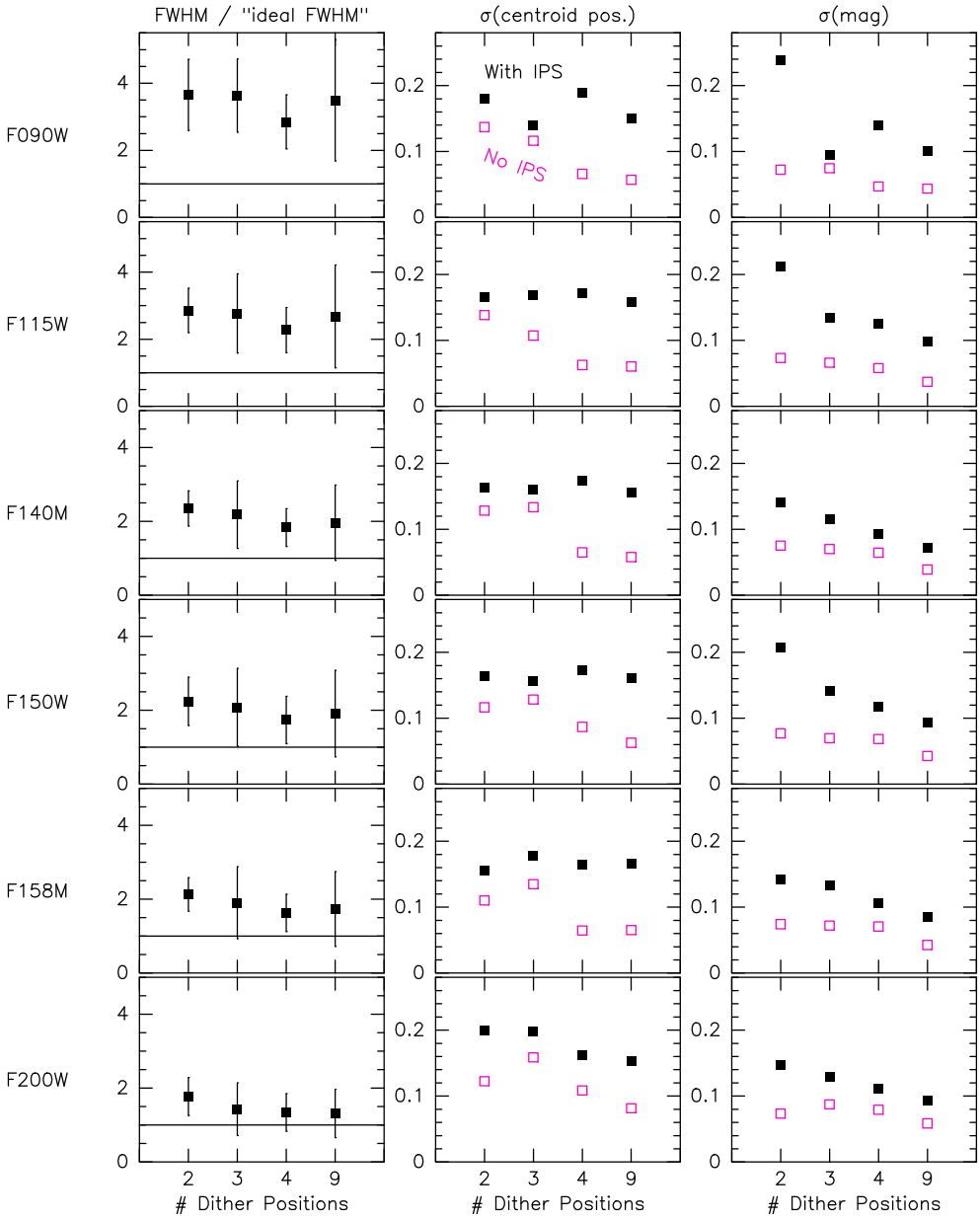

Figure 2: Results for the three "quality metrics" for FWHM, astrometry, and photometry for the four sub-pixel dither patterns considered in this study, for the 6 NIRISS filters with central wavelengths ≤ 2 μm (for which the images are undersampled by a factor ≥ 2). The first column shows the measured FWHM relative to the FWHM that a critically sampled image would have at the central wavelength of the filter in question. The second and third columns show the dispersions of the measured centroids (in pix) and photometry (in mag), respectively, relative to the known (input) values. The black squares show results with intra-pixel sensitivity (IPS) taken into account, while the ruby red open squares show the results in the absence of IPS (only one symbol is shown for FWHM since the two results are practically identical). In general, performance improves with the number of sub-pixel dithers although the 4-pt pattern is only slightly outperformed by the 9-pt pattern. Note that the results for the case without IPS are often significantly better than those for the case with IPS, highlighting the negative impact of significant IPS to imaging of undersampled PSFs.

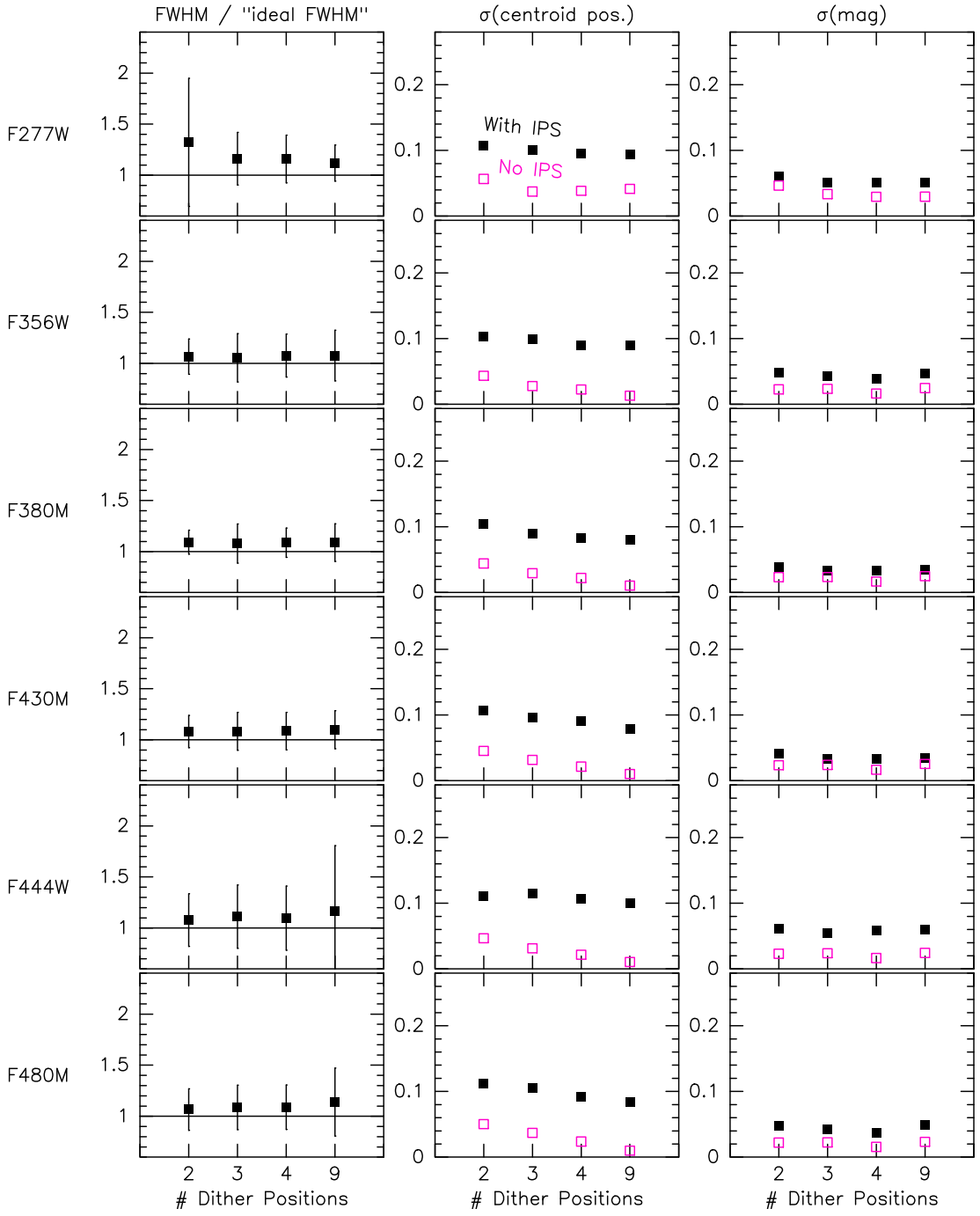

Figure 3: Similar to Figure 2, but now for the 6 NIRISS filters with central wavelength > 2 µm. The results are similar to those of the filters at ≤ 2 µm except that the FWHMs are closer to their ideal values and the photometric and astrometric quality of the combined images are better than for the shorter wavelengths, as expected given the better sampling of the long-wavelength PSFs by the NIRISS detector. Note also that the effect of IPS to these images is only marginal in terms of photometric quality, while it is still significant for astrometry (i.e., centroid accuracy).

5.5 Results of Image Analysis

We comment on the results shown in Figures 2 & 3 in this Section. Each quality metric is discussed in turn.

- For the FWHM, there are a few relevant trends with central wavelength λ_{CEN}. For $\lambda_{CEN} < 3$ μm, the FWHM metric improves when going from 2-pt dither patterns through 3-pt and 4-pt ones, whereas 9-pt dither patterns do not improve the FWHM metric any further. It can also be seen that the "best-case" FWHM gets closer to the FWHM obtained in the case of critical sampling with increasing λ_{CEN}. Once $\lambda_{CEN} \geq 3$ μm, the FWHM becomes fully consistent with the theoretical value for the case of critical sampling at the wavelength in question, even with only 2-pt or 3-pt dither patterns.
- For astrometric fidelity, the improvement with increasing number of sub-pixel dithers is stronger than that seen for the FWHM metric, in the sense that 9-pt dither patterns result in consistently smaller centroid errors relative to 4-pt patterns. This trend is seen across all NIRISS filters, even for F480M for which the PSF is quite well sampled by the detector. It can also be seen that IPS variations have a significantly negative impact on astrometric fidelity, for all filters and dither patterns. Obviously, astrometric accuracy is quite sensitive to issues regarding spatial sampling and IPS.
- For photometric fidelity, the overall trends with λ_{CEN} and the number of sub-pixel dithers are similar to those for astrometric fidelity discussed above, with two exceptions. First and foremost, the negative impact of IPS variations on photometric fidelity is significantly smaller than that on astrometry, especially for the filters with $\lambda_{CEN} \geq 3$ μm. In other words, the ability to recover the total count rate within a few pixels from the PSF center by means of dithering and image combination is much less impacted by IPS variations than the ability to recover the centroid itself (which is affected by local details of the light profile). Secondly, the dependence of photometric accuracy to the number of sub-pixel dithers is only marginal for filters with $\lambda_{CEN} \geq 3$ μm. There is a slight improvement when going from a 2-pt to a 3-pt dither pattern, while more sub-pixel dithers do not provide any significant further improvement.

6 Evaluation of Metrics for Dither Patterns for WFSS and IMAGING modes

We perform a "cost-benefit" analysis of the results shown in §5 by comparing the scientific gains achieved by the different dither patterns with the costs associated with executing them (i.e., the extra time spent in performing telescope maneuvers, extra "dead time" during exposure sequences, and/or extra mechanism moves). We concentrate on the WFSS mode in this context, since the IMAGING mode of NIRISS is only available for calibration purposes[3]. We do this analysis for a "deep-field" WFSS observing program that was prepared for the 2012 JWST Science Operations Design Reference

[3] The IMAGING mode may however become available for parallel science (Tumlinson et al. 2014). As such, the results shown in §5 should be kept in mind for the IMAGING mode as well.

Mission (SODRM), namely program 95050 (see its details in Gordon et al. 2012). This program is comprised of 9 visits for a total exposure time of ~178 hours, using 3 filters (F140M, F158M, and F200W) and 2 grisms. For instrument overheads we use the assumptions described in Gordon et al. (2013), namely that the overhead time per exposure is 15 + 11 × NINTS seconds (where NINTS stands for the number of integrations per exposure), pupil wheel moves require 46 seconds, filter wheel moves require 53 seconds, and the overhead time associated with each dither step is 20 seconds. We note that exposure sequences in the WFSS mode are set up to minimize the number of pupil and filter wheel moves. This was done because ground testing identified the two wheel mechanisms of NIRISS as potential limitations to the overall NIRISS lifetime (especially the pupil wheel). However, if two grisms are used in an exposure sequence, the grisms *are* cycled through at each dither position (in the current implementation of WFSS operations). The latter is done to ensure that the spectra taken with the two grisms (which are oriented perpendicular to each other) are taken at the same exact target position (for each dither position), which is deemed important for the data analysis. In the WFSS mode, the pupil wheel selects filters whereas the filter wheel selects a "clear" element (for direct imaging) or one of two grisms with R = 150 (see Goudfrooij et al. 2013).

For N dither moves, the overhead time (OH) for a WFSS exposure sequence with two grisms and one given filter is as follows:

$$OH = OH_{PW} + (N+3) \times OH_{FW} + 2(N+1) \times OH_{EXP} + N \times OH_{DITH}$$

(see Figures 6 and 7 in Goudfrooij et al. 2013) where the subscripts PW, FW, EXP, and DITH stand for pupil wheel, filter wheel, exposure, and dither, respectively. The values for OH are listed in Table 2 below for a variety of values of N, both in actual duration and as a fraction of the exposure time per visit (for science). The latter is 39,174 seconds in this case, for exposures with NINTS = 1. For comparison, we also list the fractional overhead for a relatively short visit of 10,000 s of exposure time (for one filter that is).

Table 2: Cost/Benefit Evaluations: NIRISS Dither Patterns for WFSS mode

Dither Pattern	2-pt	3-pt	4-pt	9-pt	16-pt
Benefits (e.g., for filter F140M):					
FWHM metric (ratio to "ideal" FWHM)	2.35	2.18	1.84	1.90	1.8:
Astrometry metric [σ(output pixel)]*	0.16/0.13	0.16/0.13	0.16/0.07	0.16/0.07	0.16:/0.05:
Photometry metric [σ(mag)]*	0.14/0.08	0.12/0.07	0.10/0.06	0.07/0.04	0.05:/0.03:
Costs:					
Overhead (seconds)	507	632	757	1382	2257
Overhead (fraction of exp. time, LONG visit)	1.3%	1.6%	1.9%	3.5%	5.8%
Overhead (fraction of exp. time, SHORT visit)	5.0%	6.3%	7.6%	13.8%	22.6%

* First values are with "worst-case" IPS, second values are without IPS.

Note that we included a 16-pt dither pattern in Table 2; this is to represent the case where the user selects a 4-pt dither pattern in conjunction with a 4-pt "mini-mosaic" which is thought to represent a use case for very deep observations in WFSS mode. The values for

the quality metrics for astrometry and photometry for the 16-pt dither pattern represent extrapolations of the trends for the patterns with fewer dithers (and we added colons to those values to indicate that they are relatively uncertain).

As shown in Table 2, the overhead time induced by the dither patterns considered here for long WFSS exposure sequences (with a given filter) is quite small relative to the science exposure time, and stays below 6% even for a 16-pt dither pattern. On the other hand, the 16-pt pattern increases the overhead by ~65% over a 9-pt pattern, and it is unlikely that the additional science benefits compensate for this substantial overhead, even for long exposure sequences. Thus, a pattern with ~9 points seems optimal for long exposure sequences unless a lowering of the photometry error by ~ 0.01 mag (~ 1%) is crucial for the science goals, in which case one could choose more dithers.

For shorter WFSS exposure sequences, the overhead time spent on dithers obviously increases relative to the science exposure time, which changes the equation. Table 2 shows that when going from a 2-pt pattern to 3-pt and 4-pt patterns, the science benefit in terms of the photometry quality metric increases by about 13 and 25%, respectively, while the overhead time increases only by a 125-250 seconds, which is typically small relative to the exposure time. As such, a 4-pt dither pattern generally appears to be a good choice for WFSS exposure sequences with several thousands of seconds of exposure time.

Nevertheless, as always, science goals of any individual observing program may involve specific requirements, be it in terms of effective spatial resolution (i.e., FWHM), photometry quality, and/or astrometry quality. As such, we recommend that observers always consider the results in Figures 2-3 in addition to the values in Table 2 before making a decision on the dither pattern.

7 Specifics on Dither Patterns for WFSS and IMAGING modes

Having performed a cost-benefit analysis for NIRISS dither patterns with a variety of numbers of sub-pixel dither steps, we turn to specific considerations for the choices of the actual dither patterns for the WFSS and IMAGING modes.

7.1 WFSS Dither Patterns

The parameters of the dither patterns for the WFSS mode were developed with the following considerations in mind. Pattern steps are chosen to have sufficient spacing along both rows and columns of the detector in order to accommodate exposures with both GR150R and GR150C grisms. The latter disperse approximately along rows and columns, respectively. The selection of dither patterns for WFSS by the user will be made based on two criteria:

a) *The number of dither steps*: 2, 3, 4, 6, or 8 steps, where the first "step" represents the initial pointing. The default choice in the WFSS template in the Astronomers Proposal Tool (APT) will be 4 steps.

b) *The dither step amplitude* (Small, Medium, and Large). The default choice will be Medium.

The dither step amplitude for the "Medium" patterns (the default choice) was chosen to be ~ 0.6 arcsec, which is thought to be appropriate for extragalactic studies at moderate-to-high redshift, which is the main science case for which the WFSS mode was originally

established. The "Small" patterns use a dither step amplitude of ~0.3 arcsec, which yields a higher conservation of pixel phase sampling across the full NIRISS field of view; these will be useful for sparse fields of point (or point-like) sources. The "Large" patterns use a dither step amplitude of ~1.2 arcsec, and are envisaged to be useful for observing astronomical scenes that involve relatively large objects (e.g., relatively low-redshift galaxies).

The WFSS dither patterns with 8 steps were created with a specific goal in mind, namely to yield a relatively small ratio of exposure time spent on direct imaging divided by that spent on grism imaging, namely approximately 0.05[4]. This ratio is thought to be sufficient for science cases where deep imaging of the target field is already available and the WFSS direct images will only be necessary to provide accurate positions for astrometry and wavelength calibration. The 8-pt dither patterns consist of two 4-pt patterns that are offset from each other by about half a 4-pt dither step. While this yields dither step amplitudes that are smaller than those for the other patterns, this was seen as a minor disadvantage for slitless spectroscopy (relative to the case of direct imaging) when compared to the disadvantage of the alternative, namely the differential geometric distortion occurring when the step sizes would stay as large as those of the patterns with fewer dither points.

We tabulate the spatial offsets with respect to the "central" pointing (i.e., the aperture location in the SIAF file) for the WFSS patterns in Tables A1-A3 in Appendix A below. (Note that pattern *names* are placeholders for now, these still require OSS review.) As an example, the dither patterns listed in Table A2 are illustrated in Figure 4 below.

It is foreseen that a significant number of science programs will use the WFSS dither patterns in conjunction with small-scale "mini-mosaics" which will perform telescope offsets of ~half a dither step along an angle of ~45° with respect to the detector rows and columns; the WFSS exposure sequences (including their dither patterns) will then be executed at each of those mini-mosaic steps. Specifics of the latter will be reported elsewhere.

7.2 IMAGING Dither Patterns

As mentioned in §6 above, the IMAGING mode of NIRISS will not be available for general observer (GO) use (mainly because the direct imaging capabilities of NIRCam surpass those of NIRISS in all relevant respects). However, it *is* possible that its use will be allowed for science parallel visits in the future, and it *will* be used for various calibration activities. To perform the latter properly, it will be important to involve dithering. To this end we prepared a set of three relatively simple dither patterns (with 2, 3, and 4 dither steps) similar to those mentioned in Table 1 (see §5.3.1) to mitigate the effects of bad pixels, intra-pixel sensitivity variations, persistence, and background level variations. These are tabulated in Table B1 in Appendix B, and illustrated in Figure 5.

[4] WFSS exposure sequences include two direct image exposures (for a given filter), namely at the first and last dither positions (see Goudfrooij et al. 2013).

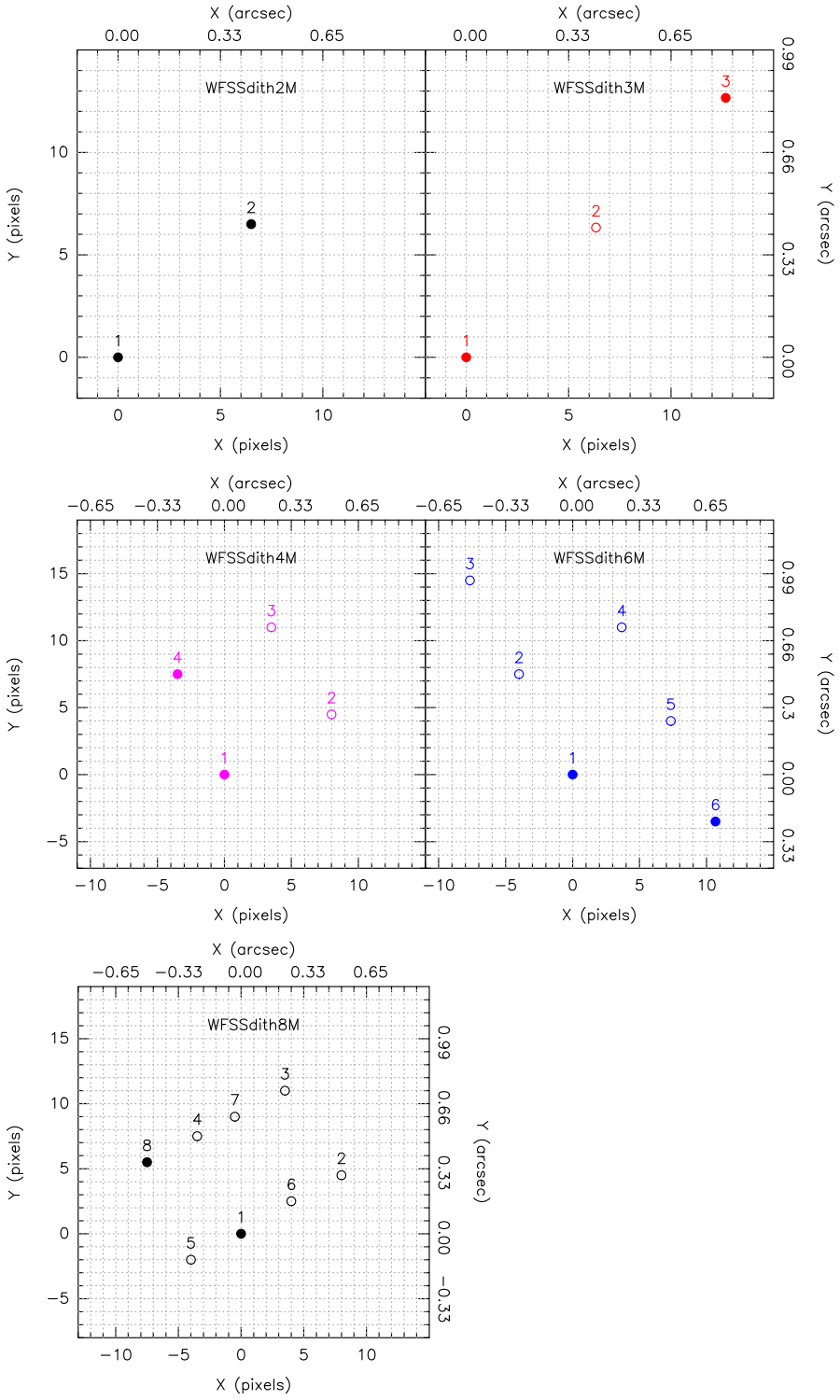

Figure 4: NIRISS/WFSS "Medium" dither patterns with ~0.6 arcsec dither steps. The label above each dither step indicates the step number (cf. Tables A1-A3). Filled circles indicate positions where direct images will be taken in addition to grism images. Preliminary dither pattern names are mentioned near the top center of each panel. The 8-pt dither pattern has smaller steps (see §7.1).

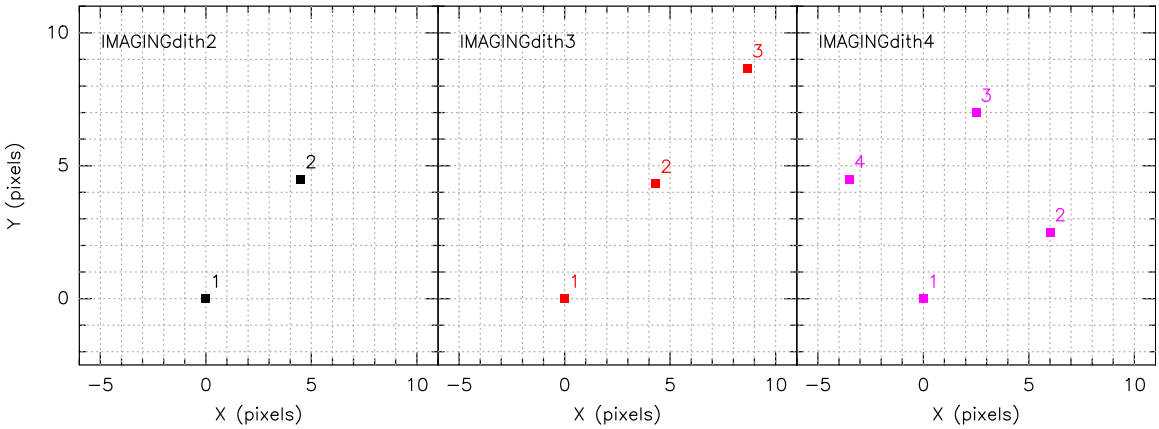

Figure 5: Illustration of the dither patterns for the IMAGING mode. The label to the top right of each filled square indicates the dither step number.

Acknowledgments

Special thanks are due to Chris Willott (NRC Herzberg) for his significant help in selecting parameters of dither patterns for the WFSS mode. Swara Ravindranath is acknowledged for preparing the APT file on SODRM program 95050, used in §6.

8 References

Ferguson, H. C., 2000, *"Science Drivers for NGST Small-Angle Maneuvers"*, STScI-NGST-R-002A (Issue A, 19 April 2000)

Fruchter, A. S., & Hook, R. N., 1997, *"Novel Linear Reconstruction Method applied to deep Hubble Space Telescope Images"*, Proc. SPIE, Vol. 3164, pp. 120-125

Fruchter, A. S., & Hook, R. N., 2002, *"Drizzle: A Method for the Linear Reconstruction of Undersampled Images"*, Publ. Astron. Soc. Pac., 114, 144

Fruchter, A. S., Sosey, M., Hack, W., et al., 2009, *"The MultiDrizzle Handbook, v3.0"* (Baltimore: STScI)

Gonzaga, S., Hack, W., Fruchter, A., & Mack, J., eds., 2012, *"The DrizzlePac Handbook"* (Baltimore: STScI)

Gordon, K. D., et al., 2012, *"Science Operations Design Reference Mission"*, JWST Technical Report JWST-STScI-000045, Rev. C

Gordon, K. D., et al., 2013, *"JWST Observatory and Instrument Overheads"*, JWST Technical Report JWST-STScI-002564

Goudfrooij, P., Fullerton, A., Dixon, V., et al. 2013, *"NIRISS Operations Concepts: The Wide Field Slitless Spectroscopy mode"*, JWST Technical Report JWST-STScI-003262

Goudfrooij, P., Artigau, E., Sivaramakrishnan, A., et al. 2014a, *"NIRISS Operations Concepts: The Aperture Masking Interferometry mode"*, JWST Technical Report JWST-STScI-003576

Goudfrooij, P., Albert, L., et al. 2014b, *"NIRISS Operations Concepts: The Single-Object*

Slitless Spectroscopy mode", JWST Technical Report JWST-STScI-003577

Goudfrooij, P., et al., 2015, *"Near Infrared Imager and Slitless Spectrograph Operations Concept Document"*, CSA-JWST-CD-0003, interim URL available upon request from P. Goudfrooij (goudfroo at stsci dot edu).

Goudfrooij, P., Albert, L., & Doyon, R., 2015, *"The Single-Object Slitless Spectrocopy Mode of Webb's NIRISS Instrument"*, STScI Newsletter, Vol. 32, Issue 1, p. 37

Hardy, T., Willott, C., & Pazder, J., 2014, *"Intra-pixel response of the new JWST infrared detector arrays"*, in High Energy, Optical, and Infrared Detectors for Astronomy VI, eds. A. D. Holland & J. Beletic, Proc. SPIE, Vol. 9154, 91542D

Koekemoer, A. M., & Lindsay, K., 2005, *"An Investigation of Optimal Dither Strategies for JWST"*, JWST-STScI-000647

Koekemoer, A. M., Fruchter, A. S., Hook, R. N., & Hack, W., 2002, *"MultiDrizzle: An Integrated Pyraf Script for Registering, Cleaning and Combining Images"*, 2002 HST Calibration Workshop, eds. S. Arribas, A. M. Koekemoer, & B. C. Whitmore (Baltimore: STScI), p. 337

Lauer, T. R., 1999a, *"Combining Undersampled Dithered Images"*, Publ. Astron. Soc. Pac., 111, 227

Lauer, T. R., 1999b, *"The Photometry of Undersampled Point-Spread Functions"*, Publ. Astron. Soc. Pac., 111, 1434

Martel, A., & Fullerton, A. W., 2013, *"The Geometric Distortion of NIRISS"*, JWST Technical Report JWST-STScI-003524

Perrin, M. D., Sivaramakrishnan, A., Lajoie, C.-P., Elliott, E., Pueyo, L., Ravindranath, S., & Albert, L., 2014, *"Updated point-spead function simulations for JWST with WebbPSF"*, Proc. SPIE 9143

Stetson, P. B., 1987, "*DAOPHOT – A Computer Program for Crowded-Field Stellar Photometry"*, Publ. Astron. Soc. Pac., 99, 191

Tumlinson, J., et al., 2014, *"JWST Science Parallels: Science Use Case and An Approach to Implementation"*, JWST Technical Report JWST-STScI-003971

Appendix A. Dither Pattern Tables for NIRISS/WFSS observing mode

Table A1. Properties of the "Small" Dither Patterns for the WFSS mode.

Pattern Name	Step #	Δx [pixels]	Δy [pixels]	ΔX [arcsec]	ΔY [arcsec]
WFSSdith2S					
	1	0.000	0.000	0.0000	0.0000
	2	3.500	3.500	0.2289	0.2303
WFSSdith3S					
	1	0.000	0.000	0.0000	0.0000
	2	4.333	4.333	0.2833	0.2851
	3	8.667	8.667	0.5668	0.5703
WFSSdith4S					
	1	0.000	0.000	0.000	0.000
	2	5.000	2.500	0.3270	0.1645
	3	2.500	6.000	0.1635	0.3948
	4	−2.500	4.500	−0.1635	0.2961
WFSSdith6S					
	1	0.000	0.000	0.0000	0.0000
	2	−2.000	3.500	−0.1308	0.2303
	3	−4.667	8.500	−0.3052	0.5593
	4	2.667	6.000	0.1744	0.3948
	5	4.333	2.000	0.2834	0.1316
	6	6.667	−2.500	0.4360	−0.1645
WFSSdith8S					
	1	0.000	0.000	0.0000	0.0000
	2	5.000	2.500	0.3270	0.1645
	3	3.500	7.000	0.2289	0.4606
	4	-1.500	4.500	-0.0981	0.2961
	5	-2.500	-1.000	-0.1635	-0.0658
	6	2.500	1.500	0.1635	0.0987

Pattern Name	Step #	Δx [pixels]	Δy [pixels]	ΔX [arcsec]	ΔY [arcsec]
	7	1.000	6.000	0.0654	0.3948
	8	-4.000	3.500	-0.2616	0.2303

Table A2. Properties of the "Medium" Dither Patterns for the WFSS mode.

Pattern Name	Step #	Δx [pixels]	Δy [pixels]	ΔX [arcsec]	ΔY [arcsec]
WFSSdith2M					
	1	0.000	0.000	0.0000	0.0000
	2	6.500	6.500	0.4251	0.4277
WFSSdith3M					
	1	0.000	0.000	0.0000	0.0000
	2	6.333	6.333	0.4142	0.4167
	3	12.667	12.667	0.8284	0.8335
WFSSdith4M					
	1	0.000	0.000	0.000	0.000
	2	8.000	4.500	0.5232	0.2961
	3	3.500	11.000	0.2289	0.7238
	4	−3.500	7.500	−0.2289	0.4935
WFSSdith6M					
	1	0.000	0.000	0.0000	0.0000
	2	−4.000	7.500	−0.2616	0.4935
	3	−7.667	14.500	−0.5014	0.9541
	4	3.667	11.000	0.2398	0.7238
	5	7.333	4.000	0.4796	0.2632
	6	10.667	−3.500	0.6976	−0.2303
WFSSdith8M					
	1	0.000	0.000	0.0000	0.0000
	2	8.000	4.500	0.5232	0.2961
	3	3.500	11.000	0.2289	0.7238
	4	-3.500	7.500	-0.2289	0.4935

Pattern Name	Step #	Δx [pixels]	Δy [pixels]	ΔX [arcsec]	ΔY [arcsec]
	5	-4.000	-2.000	-0.2616	-0.1316
	6	4.000	2.500	0.2616	0.1645
	7	-0.500	9.000	-0.0327	0.5922
	8	-7.500	5.500	-0.4905	0.3619

Table A3. Properties of the "Large" Dither Patterns for the WFSS mode.

Pattern Name	Step #	Δx [pixels]	Δy [pixels]	ΔX [arcsec]	ΔY [arcsec]
WFSSdith2L					
	1	0.000	0.000	0.0000	0.0000
	2	12.500	12.500	0.8175	0.8225
WFSSdith3L					
	1	0.000	0.000	0.0000	0.0000
	2	12.333	12.333	0.8066	0.8115
	3	24.667	24.667	1.6132	1.6231
WFSSdith4L					
	1	0.000	0.000	0.000	0.000
	2	16.000	8.500	1.0464	0.5593
	3	7.500	22.000	0.4905	1.4476
	4	−7.500	15.500	−0.4905	1.0199
WFSSdith6L					
	1	0.000	0.000	0.0000	0.0000
	2	−8.000	14.500	−0.5232	0.9541
	3	−14.667	28.500	−0.9592	1.8753
	4	6.667	22.000	0.4360	1.4476
	5	14.333	8.000	0.9374	0.5264
	6	20.667	−7.500	1.3516	−0.4935
WFSSdith8L					
	1	0.000	0.000	0.0000	0.000
	2	16.000	8.500	1.0464	0.5593

Pattern Name	Step #	Δx [pixels]	Δy [pixels]	ΔX [arcsec]	ΔY [arcsec]
	3	7.500	22.000	0.4905	1.4476
	4	-7.500	15.500	-0.4905	1.0199
	5	-8.000	-4.000	-0.5232	-0.2632
	6	8.000	4.500	0.5232	0.2961
	7	-0.500	18.000	-0.0327	1.1844
	8	-15.500	11.500	-1.0137	0.7537

Appendix B. Dither Pattern Tables for NIRISS/IMAGING observing mode

Table B1. Properties of the Dither Patterns for the IMAGING mode.

Pattern Name	Step #	Δx [pixels]	Δy [pixels]	ΔX [arcsec]	ΔY [arcsec]
IMAGINGdith2					
	1	0.000	0.000	0.0000	0.0000
	2	4.500	4.500	0.2943	0.2961
IMAGINGdith3					
	1	0.000	0.000	0.0000	0.0000
	2	4.333	4.333	0.2832	0.2849
	3	8.667	8.667	0.5670	0.5705
IMAGINGdith4					
	1	0.000	0.000	0.000	0.000
	2	6.000	2.500	0.5232	0.2961
	3	2.500	7.000	0.2289	0.7238
	4	−3.500	4.500	−0.2289	0.4935